HOKKAIDO UNIVERSITY

Title	Turbulent flame propagation mechanism of polymethylmethacrylate particle cloud-ammonia co-combustion
Author(s)	Xia, Yu; Hashimoto, Nozomu; Fujita, Osamu
Citation	Combustion and flame, 241, 112077 https://doi.org/10.1016/j.combustflame.2022.112077
Issue Date	2022-07
Doc URL	https://hdl.handle.net/2115/91384
Rights	© <2022>. This manuscript version is made available under the CC-BY-NC-ND 4.0 license http://creativecommons.org/licenses/by-nc-nd/4.0/
Rights(URL)	https://creativecommons.org/licenses/by-nc-nd/4.0/
Type	journal article
File Information	Revised manuscript.pdf

[Title page]

1. Title: Turbulent flame propagation mechanism of polymethylmethacrylate particle cloud–ammonia co-combustion

2. Author(s): Yu Xia [a], Nozomu Hashimoto [a, *], Osamu Fujita [a]

Division of Mechanical and Space Engineering, Hokkaido University,

Kita13 Nishi8, Kita-ku, Sapporo 060-8628, Japan

3. Corresponding author information:

Nozomu Hashimoto*

Professor, Hokkaido University,

Kita13 Nishi8, Kita-ku, Sapporo 060-8628, Japan

E-mail address: nozomu.hashimoto@eng.hokudai.ac.jp

Tel.: +81-11-706-6386

Fax: +81-11-706-7841

Abstract

Ammonia is a promising energy carrier for realizing a carbon-free society. In particular, solid particle cloud–ammonia co-combustion is considered as an efficient and feasible method to reduce CO_2 emissions from the thermal power generation sector by using particle-fuel such as solid waste, biomass, and pulverized coal particles in combustors. However, the fundamental turbulent flame propagation mechanism of solid particle cloud–ammonia co-combustion remains unknow. Therefore, the present study intends to investigate and validate the general turbulent flame propagation mechanism of solid particle cloud–ammonia co-combustion. To achieve this aim, silica particle cloud–ammonia–oxygen–nitrogen mixing combustion, silica particle cloud–acetylene–air mixing combustion, and PMMA particle cloud–ammonia–oxygen–nitrogen co-combustion experiments were conducted. The results showed that the turbulent flame propagation velocity of silica particle cloud–gas-fuel–oxidizer mixing combustion is lower than that of pure gas-fuel–oxidizer combustion. However, the comparison of the turbulent flame propagation velocity of PMMA particle cloud–ammonia co-combustion and that of pure ammonia combustion, showed that whether the flame propagation of the co-combustion was higher than that of the pure ammonia combustion was dependent on the equivalence ratio of the ammonia-oxidizer. Therefore, the consistency of the results between the current study of PMMA particle cloud–ammonia co-combustion and the previous study for coal particle cloud–ammonia co-combustion indicates the turbulent flame propagation mechanism of solid particle cloud–ammonia co-combustion is dominated by the negative effect of the heat sink by unburned particles and the local equivalence ratio increment effect in the preheat zone of the flame front by the addition of the volatile matter, and that the positive effect of radiation from soot particles has little effect on the turbulent flame propagation of co-combustion for small-scale flames. Further, the influence of the heterogeneous combustion of char particles on the turbulent flame propagation of solid particle cloud–ammonia co-combustion is minor because of its slow combustion

2

process. Based on the validated turbulent flame propagation mechanism of co-combustion, new numerical simulation models for solid particle cloud–ammonia co-combustion can be developed in the future.

Keywords: Solid particle cloud–ammonia–oxidizer co-combustion; Turbulent flame propagation mechanism; Inert particle effect; Radiation effect

_____

[*] Corresponding author: Tel.: +81-11-706-6386. E-mail address: nozomu.hashimoto@eng.hokudai.ac.jp

1. Introduction

The reduction of carbon dioxide (CO_2) emission is a critical issue for humankind to curb the impacts of climate change. To achieve low CO_2 emissions, the use of alternative carbon-free fuels in combustion systems is crucial. Ammonia is a promising hydrogen energy carrier and carbon-free fuel [1]. It has a high hydrogen density, can be synthesized from renewable energy sources and is easy to liquefy and store in liquid form [2]. Recently, a new ammonia production method has been proposed to realize its use as a renewable fuel [3]. Therefore, at present, ammonia combustion research has attracted much attention in the combustion community [4–8]. However, approximately 30% of the world's primary energy is currently supplied by coal-fired power generation [9]. Moreover, major challenges remain to be overcome for directly using ammonia as a fuel, such as its low combustion intensity. Although it is unlikely to completely replace coal with other fuels, the use of ammonia in thermal power plants for co-combustion is a feasible method to reduce CO_2 emissions [9–14]. Decreasing CO_2 and NO emissions in coal-fired boilers could be realized by pulverized coal–ammonia–oxidizer co-combustion [9,11]. Besides, for high-fuel-ratio coals, pulverized coal–ammonia–oxidizer co-combustion can enhance flame stability [14]. Therefore, pulverized coal particle cloud–ammonia co-combustion has immense potential and is one of the most promising ways to step into a carbon-free society. Further, co-combustion can also enable power generation from other solid particle clouds, such as solid wastes and biomass. Therefore, it is essential to investigate the characteristics and mechanism of solid particle cloud–ammonia co-combustion.

Besides, two-phase hybrid mixtures of combustible solid particles and flammable gas can be found in many industries such as mining (coal and methane), nuclear (graphite and hydrogen), pharmaceutical (pharmaceutical dust and solvent vapor), textile manufacturing (fiber and fiber vapor), and general manufacturing (organic dust and volatiles) [15]. Most of prior research on solid particle cloud–combustible-gas–diluted-oxidizer hybrid mixture co-combustion was conducted to clarify the ignition and explosion characteristics for the safety purpose in a laminar condition. Addai et al. [16] reported that the

4

addition of a small amount of flammable gas results in the decrease of the minimum ignition energy of dust. Jiang et al. [17] reported that the hybrid mixtures can be flammable when concentration of each fuel is below its lean flammability limit. Further, two key pressure-related values, namely, the maximum pressure and maximum pressure rise rate, have been studied by researchers to describe the explosion severity of hybrid-mixture co-combustion. Denkevits et al. [18]studied the effect of the addition of graphite dust to a flammable mixture of hydrogen. It was found that the maximum pressure of the hybrid mixture is higher than that derived from pure hydrogen combustion and pure graphite combustion. Dufaud et al. and Amyotte et al. [19–21] suggested that the deflagration index for hybrid mixture is higher than those of the pure gas or pure solid particle cloud. Cloney et al. [15,22,23] studied the laminar combustion regimes for hybrid mixtures.

Besides, the flame propagation velocity (or burning velocity) is a basic physical quantity for evaluating the ignition and flame stabilization performance of fuel combustion [24]. In coal-fired boilers, it is used to characterize the flame instability in the burner [25]. Moreover, for gas-fuel combustion, the burning velocity is used to characterize many combustion phenomena as it contains much physicochemical information [26]. Further, from a practical perspective, almost all combustions occur under a turbulent environment. However, the turbulent flame propagation characteristics of the two-phase hybrid mixture co-combustion was rarely studied because its complicated combustion process. Liu et al. [27] reported that the flame propagation speed and maximum flame temperature of coal dust–methane co-combustion are much higher than these of the single-coal dust flame in a laminar condition. A.S. Rangwala et al. [28–30] reported the laminar and turbulent burning velocity of hybrid (gas and dust) premixed flames by using a Bunsen burner type hybrid flame analyzer. Moreover, our research group developed a unique turbulence combustion apparatus for solid particle clouds combustion [31]. The near-homogeneous turbulence and uniform dispersion can be obtained using this combustion apparatus. Further, by using this apparatus, we discovered that, in pulverized coal–ammonia–oxygen–nitrogen co-combustion [13,14], in an ammonia-

lean case, the turbulent flame propagation velocity of co-combustion was greater than that of pure ammonia combustion. Conversely, in an ammonia-rich case, it was lower than that of pure ammonia combustion. Therefore, we explained that this phenomenon occurs based on three competing effects—the negative effect of the heat sink by unburned particles, the positive effect of radiation from soot particles in the luminous flame, and the local equivalence ratio increment effect in the preheat zone caused by the addition of the volatile matter released from the particles [13,14]. In an ammonia-lean case, the positive effects, which are the radiation effect from soot particles in the luminous flame and the local equivalence ratio increment effect in the preheat zone caused by the addition of volatile matter, are larger than the negative effect, which is heat absorption by unburned coal particles in the preheat zone. In an ammonia-rich condition, the effect of an increment of the local equivalence ratio caused by the addition of volatile matter turns into a negative effect because the addition of the fuel amount in fuel-rich cases decreases the flame temperature. Consequently, the negative effects are greater than the positive effect in an ammonia-rich condition, resulting in a lower flame propagation velocity of pulverized coal–ammonia co-combustion. However, this turbulent flame propagation mechanism was obtained using a polydispersed pulverized coal particle cloud, and it has not been verified for solid particle cloud–ammonia co-combustion systems.

As proposed by Xia et al. [13] and Hadi et al. [14], in the turbulent combustion of the pulverized coal particle cloud–ammonia–oxygen–nitrogen hybrid mixture, the heat sink effect of unburned coal particles in the preheat zone of the flame front negatively affects the turbulent flame propagation of co-combustion. However, after the reactive coal particle is heated to an elevated temperature, it releases volatile matter to induce the local equivalence ratio increment effect in the preheat zone of the flame front. Therefore, it is difficult to investigate the heat sink effect of unburned particles on the turbulent flame propagation of co-combustion using reactive particles. Instead, in a laminar condition, the inert particles such as silica particles and alumina have been suggested to decrease the flame temperature and the flame propagation

speed [32–37]. Moreover, S. Ranganathan et al. [30] reported that the effect of sand particles on the turbulent burning velocity of premixed methane–air flames under the particle concentration being lower than 0.1 kg/m^3 by using a bunsen burner type of hybrid flame analyzer. However, the effect of inert particles on the spherical turbulent flame propagation of premixed ammonia flames has not been reported to date.

Besides, as suggested by Hashimoto et al. and Hayashi et al. [38–40], soot formation in the turbulent combustion of pulverized coal affects coal particle devolatilization characteristics. Further, in pulverized coal particle cloud–ammonia co-combustion, Xia et al. [13] suggested that soot particles in the luminous flame have a radiation-positive effect to promote coal particles to release volatile matter. However, this effect has not been validated. Therefore, for the application of the co-combustion method in combustors, it is essential to validate effect of soot particles on the turbulent flame propagation mechanism of co-combustion.

Moreover, in pulverized coal particle cloud–ammonia co-combustion, coal particles follow the sequential process of heat-up, volatile matter release and combustion, soot formation, and char particle combustion. The proposed co-combustion turbulent flame propagation mechanism involves the effects of the heat sink from unburned particles in the preheat zone, the volatile matter released from the particles, and soot particles. However, the proposed mechanism has not considered the effect of the combustion of char particles. In pure solid particle cloud combustion, we clarified that the heterogeneous combustion of char particles has little effect on turbulent flame propagation because of its slow combustion process [41]. However, whether the heterogeneous combustion of char particles still plays a minor role in the turbulent flame propagation of solid particle cloud–ammonia co-combustion requires further clarification. Even though char combustion is an essential combustion process for solid particle cloud combustion in real burners, the effect of char particle reaction on the turbulent flame propagation of solid particle cloud–ammonia co-combustion has not been reported to date.

Therefore, in this study, first, the silica particle cloud–ammonia–oxygen–nitrogen mixing combustion experiments were conducted to validate the negative effect of the heat sink by unburned particles on the turbulent flame propagation of solid particle cloud–ammonia co-combustion. By using silica particle cloud, the heat sink effect from unburned particle on co-combustion can be separately analyzed by silica particle cloud–ammonia mixing combustion. Notably, in the present research, the definition of mixing combustion is different from that of co-combustion. Mixing combustion is the combustion by mixing nonreactive particles with a gas fuel–oxidizer mixture. However, co-combustion is the combustion of a hybrid mixture of gas and solid particle fuels. Second, silica particle cloud–acetylene–air mixing combustion experiments were conducted to identify the positive effect of radiation from soot particles in the luminous flame on the turbulent flame propagation of solid particle cloud–ammonia co-combustion. In acetylene-rich conditions, large-density soot particles are formed in the flame propagation process. Assuming that the negative heat sink effect of nonreactive particles is validated, under the condition of the mixing combustion of acetylene–air with silica particles, if the turbulent flame propagation velocity of mixing combustion is larger than that of pure acetylene–air combustion, the radiation has a considerable effect on the turbulent flame propagation mechanism of co-combustion. Conversely, if it is lower than that of pure acetylene–air combustion, the radiation plays a minor role in the turbulent flame propagation mechanism of co-combustion. Third, different material particles have different combustion characteristics. To investigate the effect of the heterogeneous reaction of char particles on solid particle cloud–ammonia co-combustion and the general mechanism of solid particle cloud–ammonia co-commbustion, polymethylmethacrylate (PMMA) particle cloud–ammonia co-combustion experiments were conducted under various ammonia equivalence ratios and turbulence intensities. PMMA solid particles can be decomposed to methyl methacrylate (MMA) at elevated temperature [42]; i.e., i) no heterogeneous combustion mode exists, such as char particle combustion; ii) the particle size distribution can be easily controlled and measured [43]. Finally, through above experiments, the turbulent flame propagation

mechanism of solid particle cloud–ammonia co-combustion was clarified in this research, which leads to the development of new co-combustion numerical simulation models.

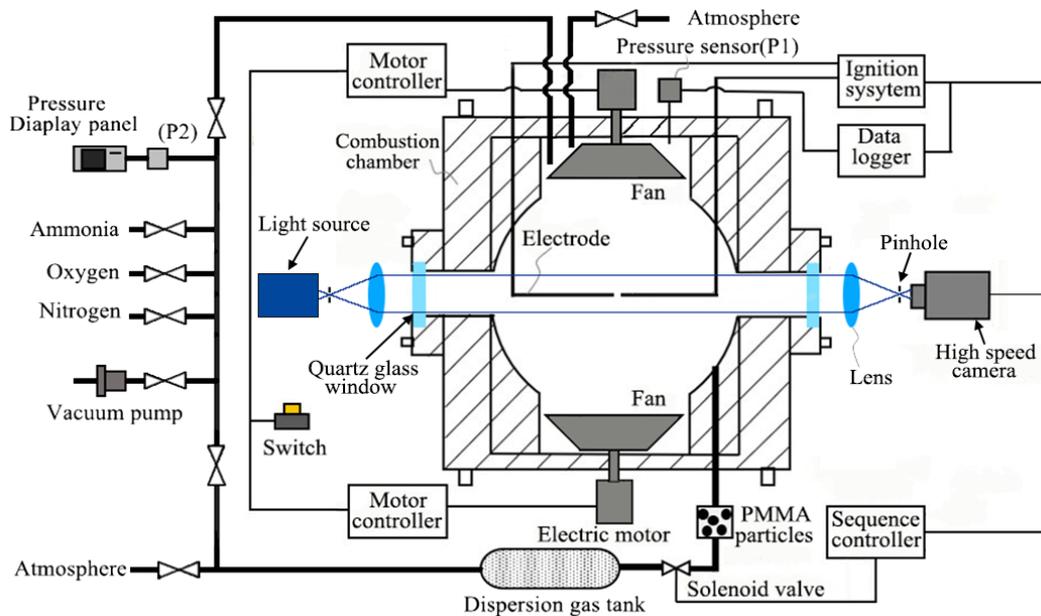## 2. Experimental setup and methods

2.1. Experimental apparatus

Fig. 1 Schematic of the experimental system.

The experimental setup is depicted in Fig. 1. Experiments were conducted using a constant-volume combustion chamber with an inside diameter of 200 mm and a height of 280 mm. The total volume of the chamber was 6.19×10^{-3} m^3. Four 50-mm-diameter optical quartz glass windows were mounted opposite to each other in the chamber for the observation of the combustion phenomenon. These optical windows were installed opposite to each other. A capacitor discharge ignition (CDI) circuit system with an ignition energy of 5.5 J was adapted to ignite the mixture. To facilitate the observation of the combustion,

electrodes were mounted at a 45° angle with respect to the interrogation path. A detailed description of the experimental setup is provided in our previous studies [2,6,31].

Turbulence was generated by two identical counter-rotation seven-bladed fans mounted vertically and symmetrically at the top and bottom of the chamber. Each fan, which was rotated by directly coupled electric motors (Maxon Motor, RE50) with separate speed controllers (Maxon Motor, ESCON 50/5), can be precisely adjustable between 0 and 15000 rpm. The fan rotation speed error was within ± 1 rpm. Turbulence characteristics were measured by particle image velocimetry (PIV) (explained in the Appendix—PIV measurement [6,31]). As a result of PIV measurements, we found that, within the central region of the vessel, the turbulence was isotropic, and there was almost no regular bulk motion [6]. Turbulence intensity, u', which was proportional to the fan speed, f_s, was found to be represented by Eq. (1):

$$u'=0.00129f_s, \tag{1}$$

where f_s is the fan rotation speed in rpm. The turbulence integral length scale, L_f, determined by two-point correlation, is 20.9 mm regardless of the turbulence intensity.

Two types of photography were used to capture turbulent flame propagation behaviors: schlieren photography and direct imaging. The detailed setting of the two photographic techniques can be seen in Fig. A in Appendix. Schlieren photography, which can capture the position of the high-density gradient caused by the rapid change in gas temperature, detects the preheat zone front of the flame front. Schlieren photography was taken by a high-speed camera (Phantom, v1212) with an LED light source (Hayashi-repic co., ltd., LA-HDF5010C). A pinhole was fixed in front of the light source to form the spotlight effect. Moreover, direct imaging was used to capture the luminous flame. The luminous flame indicates the presence of a high density of soot particles at high temperatures. These two types of photography were

explained in detail in our previous studies [6,31]. The frame rates for two high-speed cameras were set as 2500–3500 fps. The resolution setting for cameras was 512 × 512. Notably, the direct images used as a reference for the combustion phenomenon were not analyzed to obtain the flame propagation velocity because it was hard to define the border of the luminous flame front in PMMA particle cloud–ammonia co-combustion because of the weak intensity of soot particles in the flame propagation process. Furthermore, the turbulent flame propagation velocity was obtained by analyzing the schlieren photography images.

2.2. Experimental conditions

In PMMA particle cloud–ammonia–oxygen–nitrogen co-combustion, the combustion of ammonia and PMMA particles simultaneously occur in the chamber. In this study, the thermal heat input from co-combustion was kept the same as that from the pure PMMA particle cloud combustion under a certain PMMA particle concentration by theoretically subtracting a portion of the PMMA particles' thermal heat input by ammonia combustion. The total thermal heat input was calculated from the pure PMMA particle cloud combustion under a PMMA particle concentration of 0.6 kg/m^3 [13,14]. Table 1 shows the PMMA particles needed (by weight) in the co-combustion field by changing the ammonia equivalence ratio from 0 to 1.6. Additionally, the used spherical PMMA particles with a size of 30 μm had a narrow particle size distribution, which can be treated as quasi-monodispersed particles (The micrograph and size distribution data for the PMMA particles can be seen in Fig. B, Table A, and Fig. C in Appendix) [41].

Table 1
PMMA particles needed in the co-combustion field (By mass)

Ammonia equivalence ratio in the co-combustion filed ($\phi_{Ammonia}$)	PMMA particles needed in the co-combustion field to maintain the total heat input identical to 0.6 kg/m³ of PMMA particle concentration [g]
0	3.7140 (0.60)
0.2	3.3688 (0.54)
0.4	3.0843 (0.50)
0.6	2.8458 (0.46)
0.8	2.6429 (0.43)
1.0	2.4683 (0.40)
1.2	2.3163 (0.37)
1.4	2.1830 (0.35)
1.6	2.0650 (0.33)

() – Indicate the actual PMMA particle concentration in the co-combustion field, kg/m³

Further, to investigate the effect of radiation from the soot particles in the luminous flame on the turbulent flame propagation of co-combustion and simultaneously eliminate the local equivalence ratio increment effect induced by reactive particles, silica particle cloud–acetylene–air mixing combustion and the pure acetylene–air combustion experiments were conducted. The mass of silica particles used in silica particle cloud–acetylene–air mixing combustion was set to 3.714 g (which was equivalent to 0.6 kg/m³).

In silica particle cloud–ammonia–oxygen–nitrogen mixing combustion experiments, to compare with PMMA particle cloud–ammonia–oxygen–nitrogen co-combustion, silica particles with the same mass as that of the PMMA particles were used under the same ammonia equivalence ratio. Notably, silica particles were polydisperse with an average particles size of 46.08 μm. The size distribution of silica particles was measured by Microtrac MT3000 particle size analyzer. The size distribution of silica particles can be seen in Table C, Fig. D, and Table D in Appendix.

For comparison with the previous study on pulverized coal–ammonia co-combustion [13,14], the same diluted oxidizer gas mixture, composed of 40 vol.% O$_2$ and 60 vol.% N$_2$, was used for PMMA particle

cloud–ammonia co-combustion and silica particle cloud–ammonia mixing combustion.

2.3. Experimental procedures

The same experimental procedure with the pulverized coal particle cloud–ammonia–oxygen–nitrogen co-combustion [13] was used for present co-combustion and mixing combustion experiments. First, particles were equally filled into four filter cups connected to the inlets. Then, the combustion chamber and the dispersion tank were evacuated to 0 kPa by a vacuum pump. Subsequently, the dispersion tank was filled with a mixture of fuel gas, oxygen, and nitrogen. The ratios of the gases in the mixture were set based on the equivalence ratio of the fuel gas–oxidizer mixture. Similarly, the gas mixture with the same composition was supplied into the chamber. However, the gas mixture in the chamber was set to 75 kPa to ignite mixtures at 101 kPa (atmospheric pressure) after dispersion (The schematic of the dispersion system can be seen Fig. E in Appendix). The dispersion gas swept particles into the center of the spherical chamber within 0.7 s. Thereafter, 0.3 s after the dispersion ended, the mixture was ignited at atmospheric pressure [13,14,41]. The fans started to rotate for 5 min before dispersion to give the desired turbulence intensity. The initial temperature of the mixture for all experiments was set at 297 ± 3 K. The mass of particles remaining in the filter cups and tubes after the dispersion was measured to confirm the mass of particles dispersed into the chamber. After each experiment, the chamber was opened by detaching the lid, and the inner chamber was cleaned [31]. The maximum errors of the ammonia concentration, the acetylene concentration, the oxygen concentration, the pressure inside the chamber, and the PMMA/silica particle concentration were 1%, 0.5%, 1.5%, 5%, and 3%, respectively. At least three experiments were repeated for each condition to confirm the repeatability.

2.4. Particle–turbulence interactions in a homogeneous turbulence flow field

13

In this research, particles are dispersed into a homogeneous turbulence flow field. On the one hand, the turbulence characteristics maybe affected by the solid particles. Second, the particle motion is influenced by the turbulence [41].

For the turbulence modulation by particles, as illustrated by Gore and Crowe [44], the turbulence intensity of fluid might be increased by particles when the particle diameter is larger than $0.1L_f$. This criterion is widely accepted for evaluating the turbulence modulation by particles [45,46]. Therefore, for present research, the turbulence intensity might be decreased a little by the particles' interaction because the diameter of the PMMA particle used for this work is much smaller than $0.1L_f$. However, there is currently no general model that can qualitatively predict the turbulence in the particle-laden flow [41,47].

Further, for clarification of the particle motion caused by the turbulence eddies, we previously [41] calculated the Stokes number (St), which is a very important dimensionless parameter in fluid–particle flow and can be calculated by the ratio of the particle response time to the characteristic timescale of the turbulent flow [46]. The St associated with the 30 μm PMMA particle can be seen in Table E in Appendix. The results showed that the particles are well following the largest scale eddies and Taylor scale eddies. However, the particles are not well following the smallest scale eddies. However, the quantitative discussion with the particle motion in the near-homogeneous turbulence flow field is still an open question to be discussed in fluid mechanics and combustion field [47]. It is expected that the numerical simulation tool can be used for the further clarification of the particle motion in the homogeneous turbulence flow in the flame propagation process.
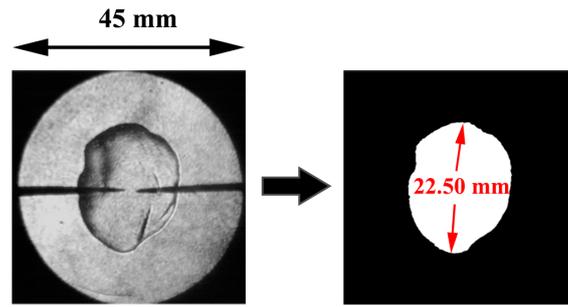
3. Flame observation and data analysis

Fig. 2 Schlieren image processing procedure.

Figure 2 shows the schlieren image processing procedure. First, the 16-bit image was processed by gray-levels from 0 = black (flame) to 255 = white (background) through applying a threshold value. Then, the processed image was transferred to the binary image in which the flame was white, and the background was black. The threshold value of the detected light intensity was selected based on visual inspection for determining the flame edge. The effect of changing the threshold value on the deviations of the flame radius and velocity was within ±2% [13, 41]. Subsequently, flame radii were measured by counting the farthest point of the flame tips. The video files of schlieren photography obtained in PMMA particle cloud–ammonia co-combustion are provided in Supplementary Materials (Video 1: $u' = 0.32$ m/s, Video 2: $u' = 0.65$ m/s, Video 3: $u' = 0.97$ m/s, Video 4: $u' = 1.29$ m/s. $\phi_{Ammonia}$ was 0.4 for all videos).
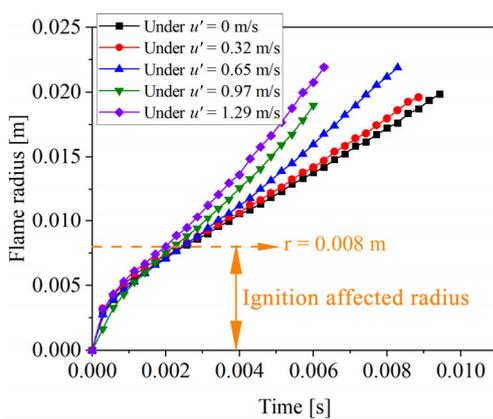
(a) Flame radius histories measured by schlieren photography
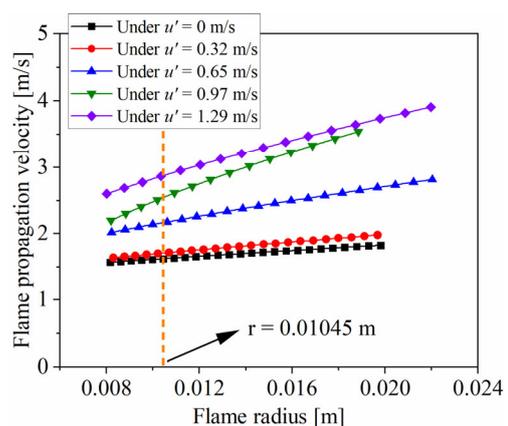
(b) Flame propagation velocity as a function of flame radius

Fig. 3 PMMA particle cloud–ammonia–oxygen–nitrogen co-combustion turbulent flame propagation under the condition of $\phi_{Ammonia} = 0.4$.

15

Figure 3(a) shows the histories of turbulent flame radius in quasi-monodispersed PMMA particle cloud–ammonia–oxygen–nitrogen co-combustion under various turbulence intensities. We previously determined the ignition-affected radius for the flame propagation using the ammonia–diluted oxygen (40% O_2, 60% N_2) mixture [2]. The results showed that the flame radius affected by the ignition energy was within 0.008 m [2]. Therefore, to eliminate the ignition-affected radius, only the flame radii data from 0.008 m to the flame front touching the window edge were used for calculating the flame propagation speed [2,13]. A polynomial relationship for the measured flame radius as a function of time was applied to obtain the turbulent flame propagation velocity. Two reasons were considered to apply polynomial relationship to the flame radius as a function of time. First, the fitted curve based on the polynomial relationship has a good satisfactory with the flame trajectory obtained by the experiment. Overall, the coefficient of determination (R-squared values) is larger than 99.5 %. Second, by applying the polynomial relationship to the flame trajectory, the turbulent flame propagation velocity can be precisely obtained by derivation with this relationship. Fig. 3(b) shows the turbulent flame propagation velocity in terms of flame radius in co-combustion. The turbulent flame propagation velocity increased with the increase in the flame radius, which was the same as that identified in our previous studies involving the turbulent combustion of pure particle clouds and pulverized coal particle cloud–ammonia–oxygen–nitrogen co-combustion [13,14,41]. The turbulent flame propagation velocity at a flame radius of 0.01045 m ($L_f/2$) was chosen for comparison. This methodology has been widely used in many solid particle and gas fuels combustion studies [2,13,14,31,48]. The flame radius of 0.01045 m was chosen because it is equivalent to the flame diameter of 0.0209 m, which is the same length as the longitudinal length scale, L_f. The longitudinal length scale was used to characterize the largest-scale eddies of the turbulence flow field.

4. Results and discussion

4.1. Negative effect of the heat sink by unburned particles on solid particle cloud–ammonia co-combustion
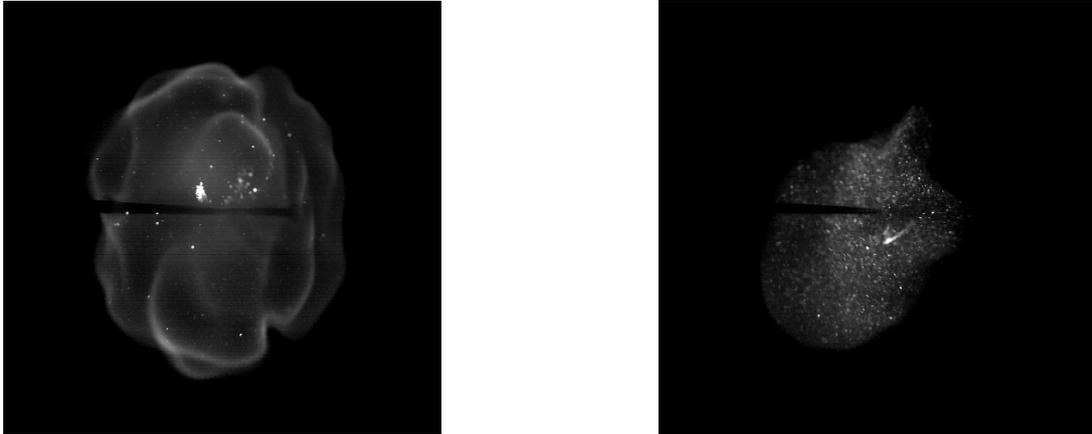
(a) Pure ammonia–oxygen–nitrogen flame under ϕ = 1.4 and u' = 0.65 m/s

(b) Silica particle cloud–ammonia mixing combustion flame under ϕ = 1.4 and u' = 0.65 m/s

Fig. 4 Direct imaging flames at the same elapsed time after ignition (0.0110 s after ignition) under pure ammonia combustion and silica particle cloud–ammonia mixing combustion.

Figure 4 shows that the direct imaging flames for pure ammonia–oxygen–nitrogen combustion and silica particle cloud–ammonia–oxygen–nitrogen mixing combustion under the same elapsed time after ignition. The video files of direct imaging are available in Supplementary Materials (Video 5: pure ammonia–oxygen–nitrogen combustion, Video 6: silica particle cloud–ammonia–oxygen–nitrogen mixing combustion.). As pointed out by Hayakawa et al. [4], the flame observed in pure ammonia combustion is caused by the NH_2 ammonia α band spectra and the superheated H_2O vapor spectra. NH_2 increases as the equivalence ratio increases. As shown in Fig. 4, under the same elapsed time, the flame radius obtained in silica particle cloud–ammonia–nitrogen mixing combustion is lower than that in pure ammonia–oxygen–nitrogen combustion. This is considered to be caused by the particles' heat sink effect. Further, light spots can be seen in the flame, as shown in Fig. 4(b). In the flame, the flame temperature is high. After the silica particles were preheated to a high temperature, they were visible as bright spots. However, the radiation from the hot silica particles has little effect on the turbulent flame propagation.

This is because, overall, the flame propagation velocity of ammonia combustion is decreased by the addition of silica particles.
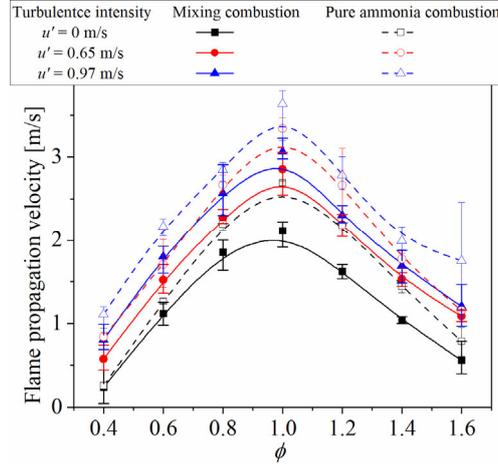

Fig. 5 Turbulent flame propagation velocity in silica particle cloud–ammonia–oxygen–nitrogen mixing combustion and pure ammonia–oxygen–nitrogen combustion under various ammonia equivalence ratios and turbulence intensities.

Figure 5 shows the turbulent flame propagation velocity of silica particle cloud–ammonia–oxygen–nitrogen mixing combustion as a function of ammonia equivalence ratio under various turbulence intensities, which was obtained by schlieren photography. Notably, the turbulent flame propagation velocity of pure ammonia–oxygen–nitrogen combustion in terms of ϕ under various turbulence intensities was also plotted in Fig. 5 [2,13].

To examine the silica particles' effect on pure ammonia–oxygen–nitrogen combustion, R was calculated by Eq. (2):

$$R = \frac{S_{Mix} - S_A}{S_A}, \qquad (2)$$

where S_{Mix} represents the turbulent flame propagation velocity in the mixing combustion, which is shown in Fig. 5 by the solid line. S_A represents the turbulent flame propagation velocity of pure ammonia–

18

oxygen–nitrogen combustion under the turbulence intensity and ammonia equivalence ratio same as those of the mixing combustion. The relation between S_A and ϕ is shown in Fig. 5 by the dotted line [13].
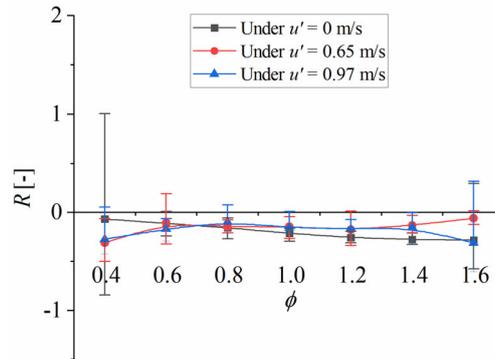

Fig. 6 R as a function of ϕ in silica particle cloud–ammonia–oxygen–nitrogen mixing combustion.

As shown in Fig. 6, all values of R are lower than 0, indicating that turbulent flame propagation velocity of silica particle cloud–ammonia–oxygen–nitrogen mixing combustion is lower than that of pure ammonia–oxygen–nitrogen combustion under the same ammonia equivalence ratio and turbulence intensity. Therefore, in silica particle cloud–ammonia–oxygen–nitrogen mixing combustion, the silica particles absorb heat from the flame. Consequently, the flame temperature is decreased, and the flame speed is lower than that of pure ammonia–oxygen–nitrogen combustion.

In the solid particle cloud–ammonia–oxygen–nitrogen co-combustion, on the one hand, the unburned reactive particles in the preheat zone of the flame front will absorb heat from the flame because the heat transfers between the high-temperature flame and the lower-temperature unburned particles to induce the thermal heat sink effect (sensible heat). On the other hand, the heat required for the devolatilization of the reactive particles is absorbed by the particles to release the volatile matter. Finally, in solid particle cloud–ammonia–oxygen–nitrogen co-combustion, the unburned particles in the preheat zone of the flame front induce the negative heat sink effect on the turbulent flame propagation of co-combustion.

4.2. Effect of radiation from soot particles in the luminous flame on the turbulent flame propagation of solid particle cloud–ammonia co-combustion


(a) Acetylene–air flame under ϕ = 3.0 and u' = 0.65 m/s

(b) Silica particle cloud–acetylene–air flame under ϕ = 3.0 and u' = 0.65 m/s

Fig. 7 Direct imaging flames at the same elapsed time (0.0053 s after ignition) for pure acetylene–air combustion and silica particle cloud–acetylene–air mixing combustion under ϕ = 3.0 and u' = 0.65 m/s

The silica particle cloud–acetylene–air mixing combustion experiments were conducted under various acetylene equivalence ratios at the same turbulence intensity (0.65 m/s). Fig. 7 shows the flames for pure acetylene–air combustion and silica particle cloud–acetylene–air mixing combustion obtained by direct imaging under the same elapsed time. The video files of direct imaging results are available in Supplementary Materials (Video 7: pure acetylene–air combustion, Video 8: silica particle cloud–acetylene–air mixing combustion.). As shown in Fig. 7(a), owing to the high-density soot particles formed during flame propagation, the luminous flame occurs in acetylene-rich combustion. Notably, the direct imaging flames shown in Figs. 4 and 7 were taken by the same camera setting. Comparing Fig. 7(a) and Fig. 4(a), we found that the light intensity from acetylene–air combustion was much stronger than that from pure ammonia combustion. Therefore, in acetylene–air combustion at a fuel-rich condition, high-density soot particles formed during flame propagation inducing the radiation effect. Besides, comparing

20

Fig. 7(a) and Fig. 7(b), we found that the light intensity in silica particle cloud–acetylene–air combustion was weaker than that in pure acetylene–air combustion. Further, the flame radius in silica particle cloud–acetylene–air combustion was smaller than that in pure acetylene–air combustion.
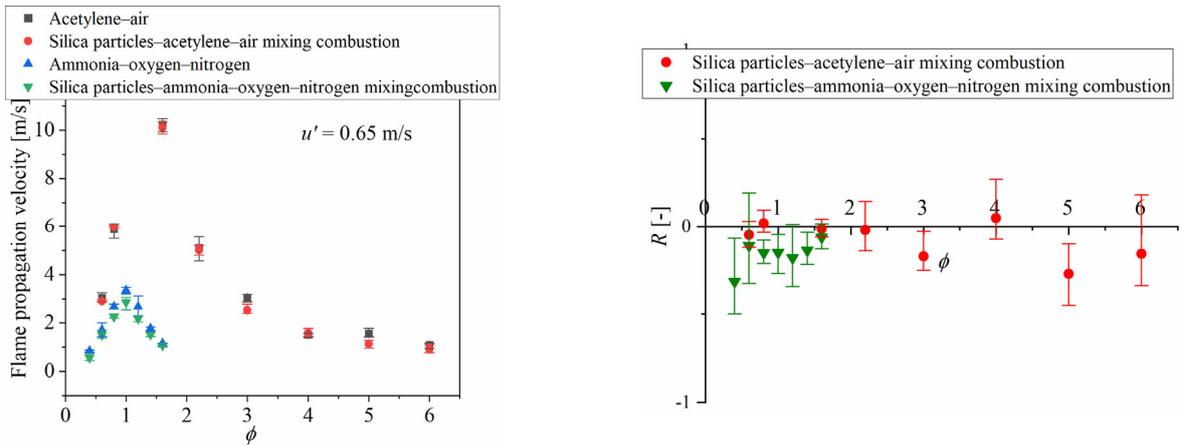
(a) Turbulent flame propagation velocity as a function of acetylene equivalence ratio in silica particle cloud–acetylene–air mixing combustion and pure acetylene–air combustion

(b) R in silica particle cloud–acetylene–air mixing combustion and silica particle cloud–ammonia–oxygen–nitrogen mixing combustion

Fig. 8 Turbulent flame propagation in silica particle cloud–acetylene–air mixing combustion and silica particle cloud–ammonia–oxygen–nitrogen mixing combustion.

Figure 8(a) shows the turbulent flame propagation velocity of silica particle cloud–acetylene–air mixing combustion and pure acetylene–air combustion as a function of acetylene equivalence ratio under a turbulence intensity of 0.65 m/s, which was obtained by schlieren photography. R, which was calculated by Eq. (2), was used to examine the impact of silica particle addition to acetylene–air combustion. Fig. 8(b) shows R as a function of the acetylene equivalence ratio. For comparison with silica particle cloud–ammonia–oxygen–nitrogen mixing combustion, the data obtained in Section 4.1. were also plotted in Figs. 8(a) and (b).

As shown in Figs. 8(a) and (b), in both silica particle cloud–ammonia–oxygen–nitrogen mixing combustion and silica particle cloud–acetylene–air mixing combustion, the turbulent flame propagation

velocity of the mixing combustion is lower than that of the pure gas combustion. Even though the acetylene–air flame forms high-density soot particles during flame propagation under acetylene-rich cases, the turbulent flame propagation velocity in silica particle cloud–acetylene–air mixing combustion is lower than that of pure acetylene–air combustion. Therefore, in silica particle cloud–acetylene–air mixing combustion, the effect of radiation from high-density soot particles cannot overcome the negative heat sink effect from the silica particles. Consequently, the turbulent flame propagation velocity is decreased by the addition of silica particles in acetylene–air combustion. Therefore, in solid particle cloud–ammonia co-combustion, the radiation heat transfer from the soot particles in the luminous flame to the solid particles in the preheat zones does not significantly affect on the turbulent flame propagation of the co-combustion.

This phenomenon is considered to be caused by the thin thickness of the flame in the study. As suggested by Hashimoto et al. [49], for the small-scale burners, the flame thickness is thinner than the large-scale burner. Furthermore, particles in a large-scale burner tend to easily obtain heat by radiation heat transfer from the large thick flame compared to that in the small test burner. Therefore, in the present study, it is concluded that the radiation plays a minor role to enhance the co-combustion turbulent flame propagation velocity for the small-scale flame. Further, it is expected that, for the large-scale flame, the radiation from high-density soot particles may strongly affect the turbulent flame propagation.

4.3. Turbulent flame propagation characteristics and mechanism of solid particle cloud–ammonia co-combustion
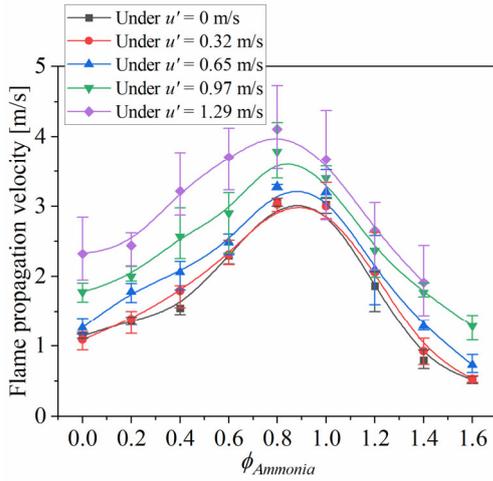
(a) Turbulent flame propagation velocity of PMMA particle cloud–ammonia–oxygen–nitrogen co-combustion as a function of $\phi_{Ammonia}$ under various turbulence intensities
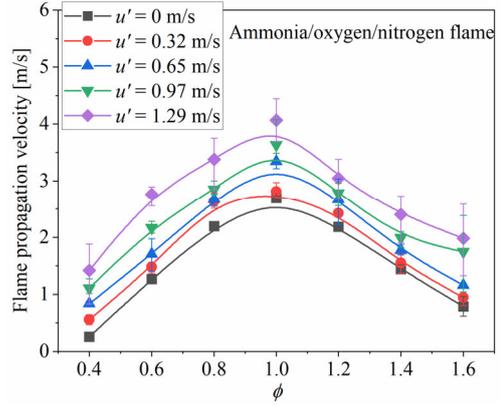
(b) Turbulent flame propagation velocity of pure ammonia–oxygen–nitrogen as a function of ϕ under various turbulence intensities [13]

Fig. 9 Turbulent flame propagation velocities of PMMA particle cloud–ammonia–oxygen–nitrogen co-combustion and pure ammonia–oxygen–nitrogen combustion

Figure 9(a) shows the turbulent flame propagation velocities of PMMA particle cloud–ammonia–oxygen–nitrogen co-combustion in terms of $\phi_{Ammonia}$ under various turbulence intensities. As shown in Fig. 9(a), the turbulent flame propagation velocity increases with the increase in the turbulence intensity. As clarified in our previous studies [13,14], this phenomenon is caused by the enhanced turbulent heat and mass transfer in the particle cloud–ammonia–oxidizer mixture and the increased total surface area of the wrinkled flame front with the increased turbulence intensity. Moreover, the turbulent flame propagation velocity first increased and then decreased with the increase in $\phi_{Ammonia}$ from 0 to 1.6. This tendency was also observed in pulverized coal particle cloud–ammonia–oxygen–nitrogen co-combustion [13].

R_P was used to characterize the impact of the PMMA particle addition on the turbulent flame propagation velocity of ammonia–oxygen–nitrogen combustion, which was calculated by Eq. (3):

$$R_P = \frac{S_{CO} - S_A}{S_A},$$ (3)

23

where S_{CO} represents the turbulent flame propagation velocity in PMMA particle cloud–ammonia–oxygen–nitrogen co-combustion, which is shown in Fig. 9(a). S_A represents the turbulent flame propagation velocity of pure ammonia–oxygen–nitrogen combustion, which is under the same turbulence intensity and ammonia equivalence ratio as those used for the co-combustion. The relation between S_A and ϕ is shown in Fig. 9(b).
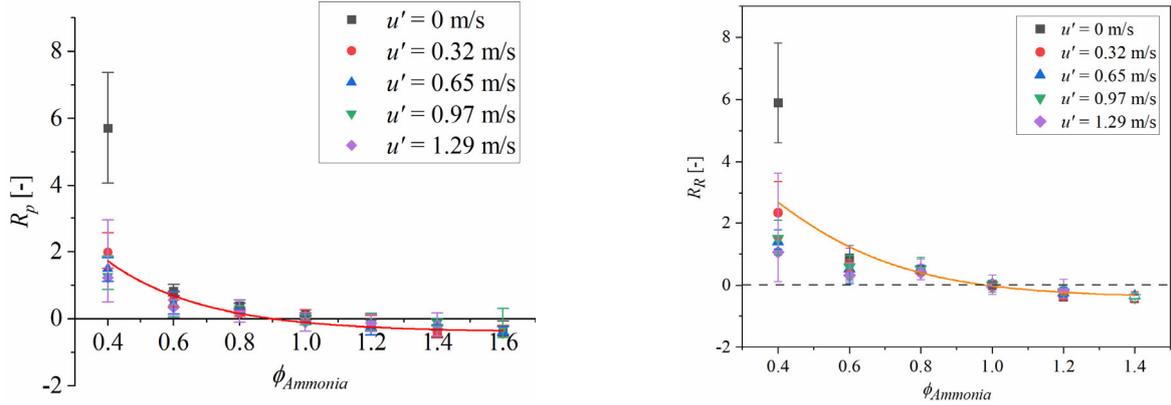
(a) R_P as a function of $\phi_{Ammonia}$ in PMMA particle cloud–ammonia–oxygen–nitrogen co-combustion under various turbulence intensities

(b) R_R as a function of $\phi_{Ammonia}$ in pulverized coal particle cloud–ammonia–oxygen–nitrogen co-combustion under various turbulence intensities [13]

Fig. 10 Impact of particle cloud on pure ammonia combustion with various solid particles.

Figure 10(a) shows R_P as a function of $\phi_{Ammonia}$ in PMMA particle cloud–ammonia–oxygen–nitrogen co-combustion under various turbulence intensities. R_P decreases with the increase in $\phi_{Ammonia}$. In ammonia-lean cases, R_P is larger than 0, indicating that the turbulent flame propagation velocity of the co-combustion is larger than that of pure ammonia–oxygen–nitrogen combustion. However, in ammonia-rich cases, the turbulent flame propagation velocity of the co-combustion is lower than that of pure ammonia–oxygen–nitrogen combustion. Fig. 10(b) shows R_R as a function of $\phi_{Ammonia}$ in pulverized coal particle cloud–ammonia–oxygen–nitrogen co-combustion, which was obtained from our previous research [13]. R_R indicted the effect of pulverized coal particle cloud on the turbulent flame propagation velocity of ammonia–oxygen–nitrogen combustion. As shown in Fig. 10 (b), the same phenomenon is observed in our previous study involving pulverized coal particle cloud–ammonia–oxygen–nitrogen co-combustion.
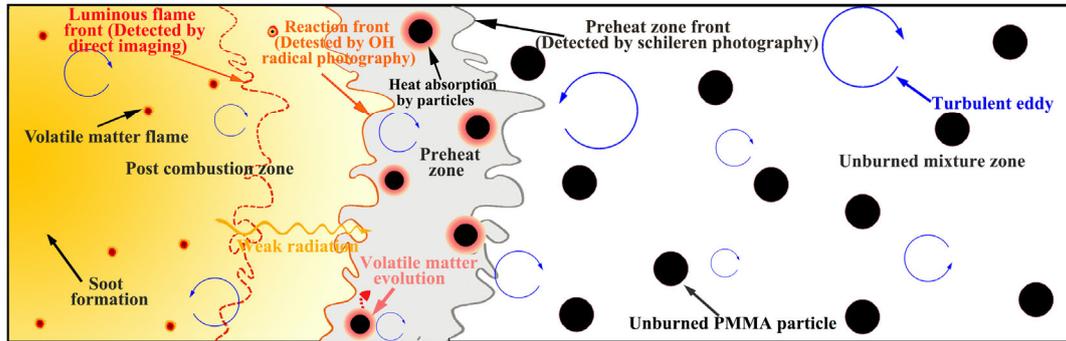
Fig. 11 Turbulent flame structure of PMMA particle cloud–ammonia–oxygen–nitrogen co-combustion.

Therefore, in the ammonia-lean case, the propagation velocity of co-combustion is larger than that of the pure ammonia combustion, while it is lower than that of pure ammonia combustion in the ammonia-rich case. Based on the consistent result between the present study and the previous study involving pulverized coal particle cloud–ammonia–oxygen–nitrogen co-combustion [13], the turbulent flame propagation mechanism of PMMA particle cloud–ammonia–oxygen–nitrogen co-combustion, which is shown in Fig. 11, was clarified. The turbulent flame of PMMA particle cloud–ammonia–oxygen–nitrogen co-combustion can be divided into three zones based on the flame propagation direction, including the post-combustion zone, the preheat zone, and the unburned mixture zone. Reactive particles have two major factors on pure ammonia combustion, including the negative effect of the heat sink by the unburned particles in the preheat zone and the local equivalence ratio increment effect in the preheat zone by the addition of volatile matter. In ammonia-lean cases, the turbulent flame propagation velocity of co-combustion was larger than that of pure ammonia combustion. This is because the positive effect, which is the increment of the local equivalence ratio by the addition of volatile matter, is larger than the negative effect, which is the heat sink effect by the unburned particles in the preheat zone of the flame front. Conversely, in ammonia-rich cases, the local equivalence ratio increment effect by the addition of volatile matter becomes negative because the addition of fuel species decreases the flame temperature.

25

Consequently, the turbulent flame propagation velocity of the co-combustion was lower than that of the pure ammonia–oxygen–nitrogen combustion in ammonia-rich cases. In the ammonia stoichiometric condition, the turbulent flame propagation velocity of the co-combustion was almost the same as that of the pure ammonia–oxygen–nitrogen combustion as the negative effect is offset by the positive effect.

Therefore, in the turbulent flame propagation of solid particle cloud–ammonia–oxygen–nitrogen co-combustion, first, the unburned particles in the preheat zone of the flame front have a negative heat sink effect. Second, the local equivalence ratio increment effect by the addition of volatile matter in the preheat zone can induce a positive or negative effect, which was determined by the ammonia equivalence ratio. Third, the effect of radiation from soot particles in the luminous flame has a minor effect on the turbulent flame propagation of co-combustion for small-scale flames.

Furthermore, the consistency of results from the current study of PMMA particle cloud–ammonia–oxygen–nitrogen co-combustion and the previous study of pulverized coal particle cloud–ammonia–oxygen–nitrogen co-combustion confirmed that the heterogeneous combustion of char particles has little effect on the turbulent flame propagation of co-combustion because of its slow combustion process.

5. Conclusions

In the present study, the fundamental turbulent flame propagation mechanism of solid particle cloud–ammonia co-combustion was investigated. Three types of experiments were conducted to investigate and validate the turbulent flame propagation mechanism of solid particle cloud–ammonia co-combustion. The silica particle cloud–ammonia–oxygen–nitrogen mixing-combustion experiments were conducted to investigate the negative effect of the heat sink by the unburned particles on the turbulent flame propagation of solid particle cloud–ammonia co-combustion. Silica particle cloud–acetylene–air mixing combustion experiments were conducted to investigate the effect of radiation from soot particles in the luminous flame on the turbulent flame propagation of solid particle cloud–ammonia–oxidizer co-combustion. Moreover,

PMMA particle cloud–ammonia–oxygen–nitrogen co-combustion experiments were conducted to validate the co-combustion mechanism studied previously and clarify the effect of char reaction on the turbulent flame propagation of co-combustion. The principal findings are as follows:

In silica particle cloud–ammonia–oxygen–nitrogen mixing combustion, the turbulent flame propagation velocity of the mixing combustion was lower than that of pure ammonia–oxygen–nitrogen combustion. Therefore, the unburned particles in the preheat zone of the flame front in solid particle cloud–ammonia–oxidizer co-combustion have a negative heat sink effect on the turbulent flame propagation.

Further, in silica particle cloud–acetylene–air mixing combustion, the turbulent flame propagation velocity of the mixing combustion was lower than that of pure acetylene–air combustion. Therefore, in solid particle cloud–ammonia co-combustion, the radiation heat transfer from the luminous flame to the particles in the preheat zone has weak effect on the flame propagation velocity of co-combustion for the small-scale flame.

The results obtained agreed well with those of the previous study on pulverized coal particle cloud–ammonia–oxygen–nitrogen co-combustion. In the ammonia-lean case, the propagation velocity of co-combustion is larger than that of the pure ammonia combustion, while it is lower than that of pure ammonia combustion in the ammonia-rich case. Therefore, the turbulent flame propagation mechanism for solid particle cloud–ammonia co-combustion is dominated by the by the negative effect of the heat sink by unburned particles and the local equivalence ratio increment effect in the preheat zone of the flame front by the addition of the volatile matter. Further, the consistency of the results between the current study of PMMA particle cloud–ammonia co-combustion and the previous study for coal particle cloud–ammonia co-combustion showed that the heterogeneous combustion of char particles has little effect on the turbulent flame propagation velocity of co-combustion because of its slow combustion process.

27

References

[1] J. Li, H. Huang, N. Kobayashi, Z. He, Y. Osaka, T. Zeng, Numerical study on effect of oxygen content in combustion air on ammonia combustion, Energy 93 (2015) 2053–2068.

[2] Y. Xia, G. Hashimoto, K. Hadi, N. Hashimoto, A. Hayakawa, H. Kobayashi, O. Fujita, Turbulent burning velocity of ammonia/oxygen/nitrogen premixed flame in O_2-enriched air condition, Fuel 268 (2020) 117383.

[3] K. Sato, K. Nagaoka, Boosting ammonia synthesis under mild reaction conditions by precise control of the basic oxideru interface, Chem. Lett. 50 (2021) 687–696.

[4] A. Hayakawa, T. Goto, R. Mimoto, Y. Arakawa, T. Kudo, H. Kobayashi, Laminar burning velocity and Markstein length of ammonia/air premixed flames at various pressures, Fuel 159 (2015) 98–106.

[5] A. Ichikawa, A. Hayakawa, Y. Kitagawa, K.D.K.A. Somarathne, T. Kudo, H. Kobayashi, Laminar burning velocity and Markstein length of ammonia/hydrogen/air premixed flames at elevated pressures, Int. J. Hydrogen Energy 40 (2015) 9570–9578.

[6] R. Ichimura, K. Hadi, N. Hashimoto, A. Hayakawa, H. Kobayashi, O. Fujita, Extinction limits of an ammonia/air flame propagating in a turbulent field, Fuel 246 (2019) 178–186.

[7] H. Kobayashi, A. Hayakawa, K.D.K.A. Somarathne, E.C. Okafor, Science and technology of ammonia combustion, Proc. Combust. Inst. 37 (2019) 109–133.

[8] E.C. Okafor, Y. Naito, S. Colson, A. Ichikawa, T. Kudo, A. Hayakawa, H. Kobayashi, Experimental and numerical study of the laminar burning velocity of CH_4–NH_3–air premixed flames, Combust. Flame 187 (2018) 185–198.

[9] J. Zhang, T. Ito, H. Ishii, S. Ishihara, T. Fujimori, Numerical investigation on ammonia co-firing in a pulverized coal combustion facility: Effect of ammonia co-firing ratio, Fuel 267 (2020) 117166.

[10] Yamamoto A, Kimoto M, Blended combustion characteristics of pulverized coal and ammonia in pulverized-coal-combustion test furnace, 55th Symppsium (Japanese) on Combustion, 2017, Toyama, Japan.

[11] S. Ishihara, J. Zhang, T. Ito, Numerical calculation with detailed chemistry of effect of ammonia co-firing on NO emissions in a coal-fired boiler, Fuel 266 (2020) 116924.

[12] Central Research Institute of Electric Power Industry, 2017, avaliable at https://criepi.denken.or.jp/press/pressrelease/2017/01_10press.pdf (In Japanese).

[13] Y. Xia, K. Hadi, G. Hashimoto, N. Hashimoto, O. Fujita, Effect of ammonia/oxygen/nitrogen equivalence ratio on spherical turbulent flame propagation of pulverized coal/ammonia co-combustion, Proc. Combust. Inst. 38 (2021) 4043–4052.

[14] K. Hadi, R. Ichimura, G. Hashimoto, Y. Xia, N. Hashimoto, O. Fujita, Effect of fuel ratio of coal on the turbulent flame speed of ammonia/coal particle cloud co-combustion at atmospheric pressure, Proc. Combust. Inst. 38 (2021) 4131–4139.

[15] C.T. Cloney, R.C. Ripley, M.J. Pegg, P.R. Amyotte, Laminar combustion regimes for hybrid mixtures of coal dust with methane gas below the gas lower flammability limit, Combust. Flame 198 (2018) 14–23.

[16] E.K. Addai, D. Gabel, M. Kamal, U. Krause, Minimum ignition energy of hybrid mixtures of combustible dusts and gases, Process Saf. Environ. Prot. 102 (2016) 503–512.

[17] J. Jiang, Study of Dust-Gas Hybrid Mixture Explosions, PhD thesis, Texas A&M University, 2015.

[18] A. Denkevits, Explosibility of hydrogen-graphite dust hybrid mixtures, J. Loss Prev. Process Ind. 20 (2007) 698–707.

[19] O. Dufaud, L. Perrin, M. Traoré, Dust/vapour explosions: Hybrid behaviours?, J. Loss Prev. Process Ind. 21 (2008) 481–484.

[20] O. Dufaud, L. Perrin, M. Traore, S. Chazelet, D. Thomas, Explosions of vapour/dust hybrid mixtures: A particular class, Powder Technol. 190 (2009) 269–273.

[21] P.R. Amyotte, R.K. Eckhoff, Dust explosion causation, prevention and mitigation: An overview, J. Chem. Heal. Saf. 17 (2010) 15–28.

[22] C.T. Cloney, R.C. Ripley, M.J. Pegg, P.R. Amyotte, Role of particle diameter in laminar combustion regimes for hybrid mixtures of coal dust and methane gas, Powder Technol. 362 (2020) 399–408.

[23] C.T. Cloney, R.C. Ripley, M.J. Pegg, P.R. Amyotte, Evaluating regime diagrams for closed volume hybrid explosions, J. Loss Prev. Process Ind. 49 (2017) 912–918.

[24] M. Taniguchi, Flame Propagation Velocity for Co-combustion of Pulverized Coals and Gas Fuels, Energy & Fuels 35 (2021) 6305–6314..

[25] T. Suda, K. Masuko, J. Sato, A. Yamamoto, K. Okazaki, Effect of carbon dioxide on flame propagation of pulverized coal clouds in CO_2/O_2 combustion, Fuel 86 (2007) 2008–2015.

[26] C.K. Law, Combustion Physics, Cambridge University Press, Cambridge, 2006.

[27] Y. Liu, J. Sun, D. Chen, Flame propagation in hybrid mixture of coal dust and methane, J. Loss Prev. Process Ind. 20 (2007) 691–697.

[28] Y. Xie, V. Raghavan, A.S. Rangwala, Study of interaction of entrained coal dust particles in lean methane-air premixed flames, Combust. Flame 159 (2012) 2449–2456.

[29] S.R. Rockwell, A.S. Rangwala, Influence of coal dust on premixed turbulent methane-air flames, Combust. Flame 160 (2013) 635–640.

[30] S. Ranganathan, D. Petrow, S.R. Rockwell, A.S. Rangwala, Turbulent burning velocity of methane–

air–dust premixed flames, Combust. Flame 188 (2018) 367–375.

[31] K. Hadi, R. Ichimura, N. Hashimoto, O. Fujita, Spherical turbulent flame propagation of pulverized coal particle clouds in an O_2/N_2 atmosphere, Proc. Combust. Inst. 37 (2019) 2935–2942.

[32] M.G. Andac, F.N. Egolfopoulos, C.S. Campbell, Effects of combustible dust clouds on the extinction behavior of strained, laminar premixed flames in normal gravity, Proc. Combust. Inst. 29 (2002) 1487–1493.

[33] Q. Li, C. Liu, H. Zhang, M. Wang, Z. Chen, Initiation and propagation of spherical premixed flames with inert solid particles, Combust. Theory Model. 24 (2020) 606–631.

[34] S. Ranganathan, M. Lee, V. Akkerman, A.S. Rangwala, Suppression of premixed flames with inert particles, J. Loss Prev. Process Ind. 35 (2015) 46–51.

[35] M. Dewitte, J. Vrebosch, A. van Tiggelen, Inhibition and extinction of premixed flames by dust particles, Combust. Flame 8 (1964) 257–266.

[36] T. Mitani, A flame inhibition theory by inert dust and spray, Combust. Flame 43 (1981) 243–253.

[37] T. Mitani, T. Niioka, Extinction phenomenon of premixed flames with alkali metal compounds, Combust. Flame 55 (1984) 13–21.

[38] N. Hashimoto, J. Hayashi, N. Nakatsuka, K. Tainaka, S. Umemoto, H. Tsuji, F. Akamatsu, H. Watanabe, H. Makino, Primary soot particle distributions in a combustion field of 4 kw pulverized coal jet burner measured by time resolved laser induced incandescence (TiRe-LII), J. Therm. Sci. Technol. 11 (2016) 1–11.

[39] J. Hayashi, N. Hashimoto, N. Nakatsuka, H. Tsuji, H. Watanabe, H. Makino, F. Akamatsu, Soot formation characteristics in a lab-scale turbulent pulverized coal flame with simultaneous planar measurements of laser induced incandescence of soot and Mie scattering of pulverized coal, Proc. Combust. Inst. 34 (2013) 2435–2443.

[40] N. Hashimoto, J. Hayashi, Coal Particle Devolatilization and Soot Formation in Pulverized Coal

Combustion Fields, KONA Powder Part. J. (2021) 1–21.

[41] Y. Xia, N. Hashimoto, O. Fujita, Turbulent flame propagation of polymethylmethacrylate particle clouds in an O_2/N_2 atmosphere, Combust. Flame 234 (2021) 111616.

[42] M. Hertzberg, I.A. Zlochower, Devolatilization wave structures and temperatures for the pyrolysis of polymethylmethacrylate, ammonium perchlorate, and coal at combustion level heat fluxes, Combust. Flame 84 (1991) 15–37.

[43] H. Kobayashi, N. Ono, Y. Okuyama, T. Niioka, Flame propagation experiment of PMMA particle cloud in a microgravity experiment, Symp. (Int.) Combust. 25 (1994) 1693–1699.

[44] R.A. Gore, C.T. Crowe, Effect of particle size on modulating turbulent intensity, Int. J. Multiph. Flow 15 (1989) 279–285.

[45] M. Mandø, Turbulence Modulation By Non-Spherical Particles, Aalborg University, 2009.

[46] C.T. Crowe, J.D. Schwarzkopf, M. Sommerfeld, Multiphase Flow in Droplets and Particles, CRC press, Boca Raton, 2011.

[47] R. Monchaux, M. Bourgoin, A. Cartellier, Analyzing preferential concentration and clustering of inertial particles in turbulence, Int. J. Multiph. Flow 40 (2012) 1–18.

[48] M. Lawes, M.P. Ormsby, C.G.W. Sheppard, R. Woolley, The turbulent burning velocity of iso-octane/air mixtures, Combust. Flame 159 (2012) 1949–1959.

[49] N. Hashimoto, H. Watanabe, Numerical analysis on effect of furnace scale on heat transfer mechanism of coal particles in pulverized coal combustion field, Fuel Process. Technol. 145 (2016) 20–30.